Available online at www.sciencedirect.com
SCIENCE DIRECT®
Energy and Buildings 36 (2004) 815–823
ENERGY and BUILDINGS
www.elsevier.com/locate/enbuild

Spatio-temporal dynamics of solar shading for a parametrically defined roof system

J. Mardaljevic*

Institute of Energy and Sustainable Development (IESD), De Montfort University, The Gateway, Leicester LE1 9BH, UK

Abstract

The evaluation of shading devices is generally carried out using a sequence of shadow-pattern images showing the progression of solar penetration for particular times of the day or year. This approach can reveal when solar penetration may occur, say at the summer solstice, but it cannot give a quantitative measure of the degree and likelihood of solar penetration over a representative period of a full year. This paper describes a new image-based technique to quantify the effectiveness of shading devices. It is founded on predictions of direct solar irradiation using hourly meteorological data for a full year. In addition to numerical output, the technique produces synoptic images that reveal the spatial and temporal variation of solar irradiation. There are no practical limits on the scene geometry and buildings with thousands of individual shading elements can be evaluated. The technique is designed to be both fast and highly scalable making it suitable for the evaluation of a large number of design variants. This is demonstrated in the paper using a parametrically defined model of a complex roof shading system based on the Changi Airport Terminal 3 design. The 3600 fins that comprise the roof shading system were generated using a parametric scheme where the fin orientation has a random component. A total of 42 design variants of the roof shading system were evaluated using the new technique.

Keywords: Solar shading; Simulation; Parametric model

1. Introduction

The usual assessment method for solar penetration is based on one or more ‘snapshot’ images showing views of the internal surfaces illuminated by direct sun at certain times of the year [1]. This can be achieved using scale models with a heliodon or be rendering-based. The images in Fig. 1 show an internal view of a ‘Drafting Office’ 3D computer model (top) and two frames from an animation sequence that was generated to show the progression of solar penetration from the rooflights and windows. The internal view and the animation were rendered using the radiance lighting simulation system [2]. The animation frames comprise pairs of images showing the sun’s view of the building (left) and the internal view from high above (right). The sequence was generated for all daylight times at 15 min intervals for the first day of each month from January to June. For the image on the right of the animation frames, the roof was eliminated from the view using a feature in radiance called ‘clipping planes’. A green ‘wash’ of ambient light was used to provide a subdued background against which the bright patches of solar penetration are clearly seen. Computer simulation offers many advantages over physical modelling approaches for the conventional shadow-pattern analysis. For example, detail can be accurately modelled at any scale; the generation of movie sequences can be automated; and, the radiance ‘clipping plane’ technique has no equivalent in physical (i.e. scale) modelling. These advantages notwithstanding, the fundamental limitations of the basic approach remain unchanged: it is essentially qualitative. The conventional assessment method can only disclose when solar penetration may occur but cannot make any quantitative measure of it.

For complex shading systems comprised of many, possibly thousands, of individual shading elements, the conventional shadow-pattern approach is unlikely to offer any meaningful basis for design evaluation. Doubly so when there are a number of design variants that need to be considered. Consider the concept-rendering of the roof shading system proposed for Changi Airport Terminal 3 in Singapore (Fig. 2). This gives a visual impression of a highly complex shading system envisaged for the terminal building by architects Skidmore, Owings & Merrill.

The precise details for the Changi roof design were not known to the author. It is understood however that, for the

* Tel.: +44-116-257-7972; fax: +44-116-257-7981.
E-mail address: jm@dmu.ac.uk (J. Mardaljevic).

0378-7788/$ – see front matter © 2004 Elsevier B.V. All rights reserved.
doi:10.1016/j.enbuild.2004.01.020

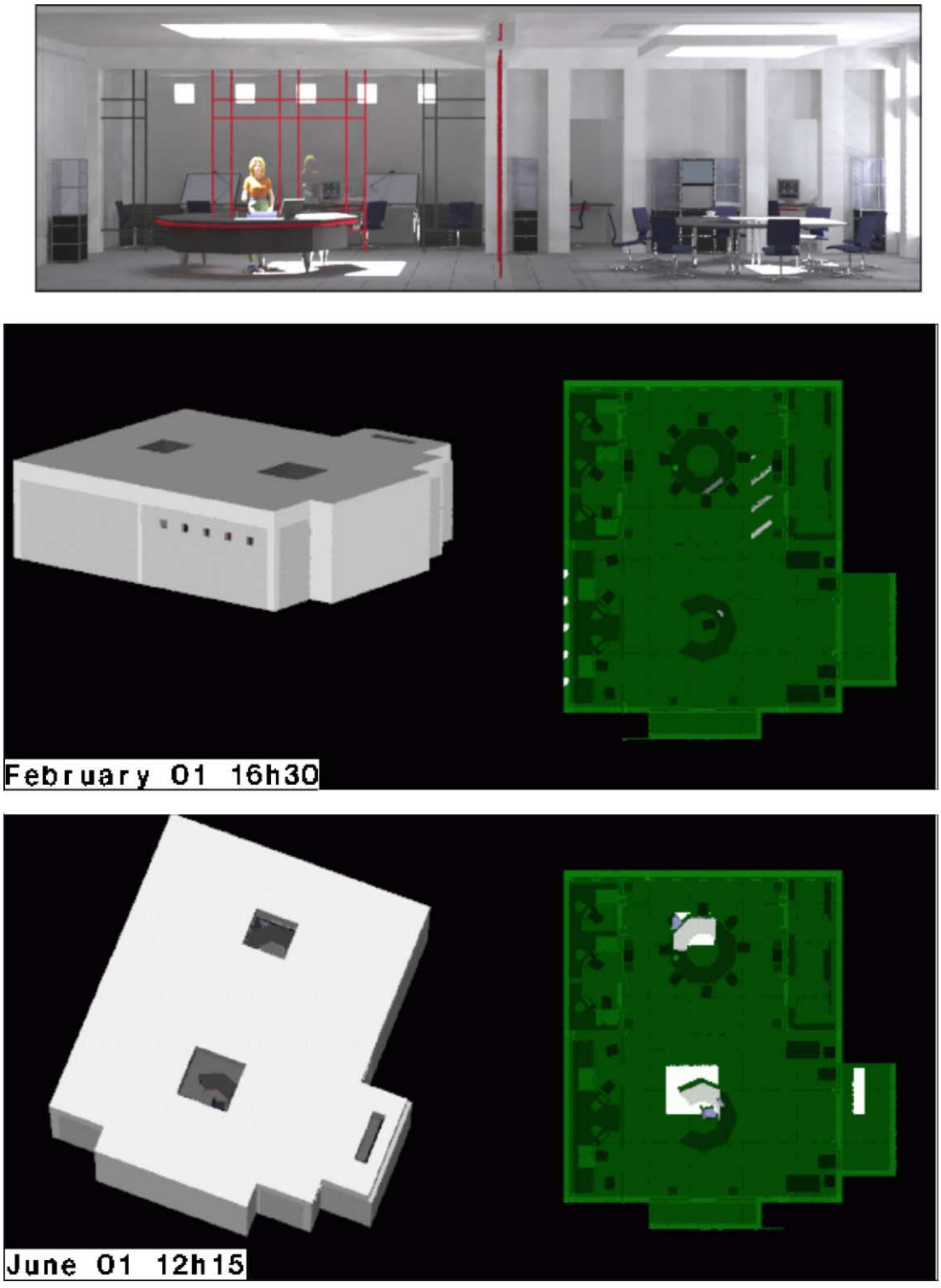

Fig. 1. Traditional approach to modelling solar penetration: generate progression of shadow patterns for various times of the day or year.

concept-rendering, a parametric scheme with a random component was used to orientate the thousands of shading fins. A critical design factor for the Changi Terminal 3 roof will have been the potential for solar gain at floor level, and the associated cooling load quantities beyond the grasp of the conventional shadow-pattern approach.

This paper describes a new technique to predict solar penetration in buildings which is founded on an image-based simulation of the total annual irradiation due to direct sun incident on internal building surfaces. The new approach has several advantages over the standard method. For example, all possible sun positions are accounted for, and, because the

Fig. 2. Rendering showing visual impression of Changi Terminal 3. Image by J. Seagull, copyright Pixel by Pixel and Skidmore, Owings & Merrill.

analysis is founded on realistic meteorological data (e.g. test reference year time-series), a quantitative measure of direct solar penetration is obtained. Thus, it is possible to make reliable quantitative comparison of two or more design variants. For this paper, the new approach was used to evaluate 42 design variants of a highly complex roof shading system similar to that envisaged for Changi Airport.

2. New approach

2.1. STIMAP

The new approach is called spatio-temporal irradiation mapping (STIMAP). The spatial map reveals the quantity and distribution of total annual direct irradiation incident on a building surface or surfaces. Whereas the temporal map shows the propensity for high instantaneous irradiation across those surfaces throughout the year. Example results from an earlier study on the effectiveness of a brise-soleil are shown in Fig. 3 [3].

The spatial map clearly shows high levels of total annual direct irradiation for some sections of the building perimeter, Fig. 3b. The propensity for solar penetration throughout the year is revealed in the temporal map, Fig. 3c. This shows that the highest levels of solar penetration will occur between the hours 17:00–19:00 h for the months April–August, and during early morning for the winter months. The propensity temporal map shows the mean solar irradiance across the floor area (or any part of it) produced by a unit (i.e. fixed) brightness sun occurring throughout the year. This is preferred to a map showing the absolute values based on TRY data because the patterns of variation in the direct normal irradiance (which are unique to the TRY) can obscure the underlying temporal pattern in the propensity for solar penetration. This is of course not an issue with the spatial map where each pixel point shows the integral of TRY-derived instantaneous irradiance over a full year.

The adoption of an image-based approach imparts significant advantages over the conventional assessment methods. In addition to providing precise, quantitative performance data, the images can be easily understood with the bare minimum of explanation. Indeed, those architects that have worked with the analyses have remarked that it is far easier to gain an insight into shading performance from STIMAP images than from the usual sequence of shading pattern images (private communication: James Nicholls, SGP Architects, UK). This is because the spatial map is, in effect, a (quantitative) cumulation of a ‘movie’ sequence of shading patterns for an entire year at a short time-step. Furthermore, the STIMAP images are more readily intelligible than the commonly used sun-path stereographic-projection charts [4].

2.2. STIMAP—theoretical basis

The total annual (direct) irradiation, or TAI, is computed using physically-based lighting simulation (i.e. rendering) techniques. The standard (UNIX) *Radiance* lighting simulation system is used as the rendering ‘engine’ in STIMAP. The *radiance* system has been rigorously validated by the author and proven to be highly accurate for daylight modelling [5]. The key to the new technique are the algorithms that allow the efficient computation of images of the total annual irradiation based on hourly (or sub-hourly) meteorological data, e.g. test reference year (TRY) (TMY in US) time-series. Using hourly values, a brute force approach would entail the computation of ∼4000 irradiation renderings—one for each hour of daylight. In STIMAP, the total annual irradiation is accurately synthesised from a much smaller number of renderings (∼200). This is achieved by transforming the problem from the time-series domain to the sun-position domain.

The transformation involves several stages. First, the above-horizon sun positions that occur annually at the location of the proposed building are computed using standard

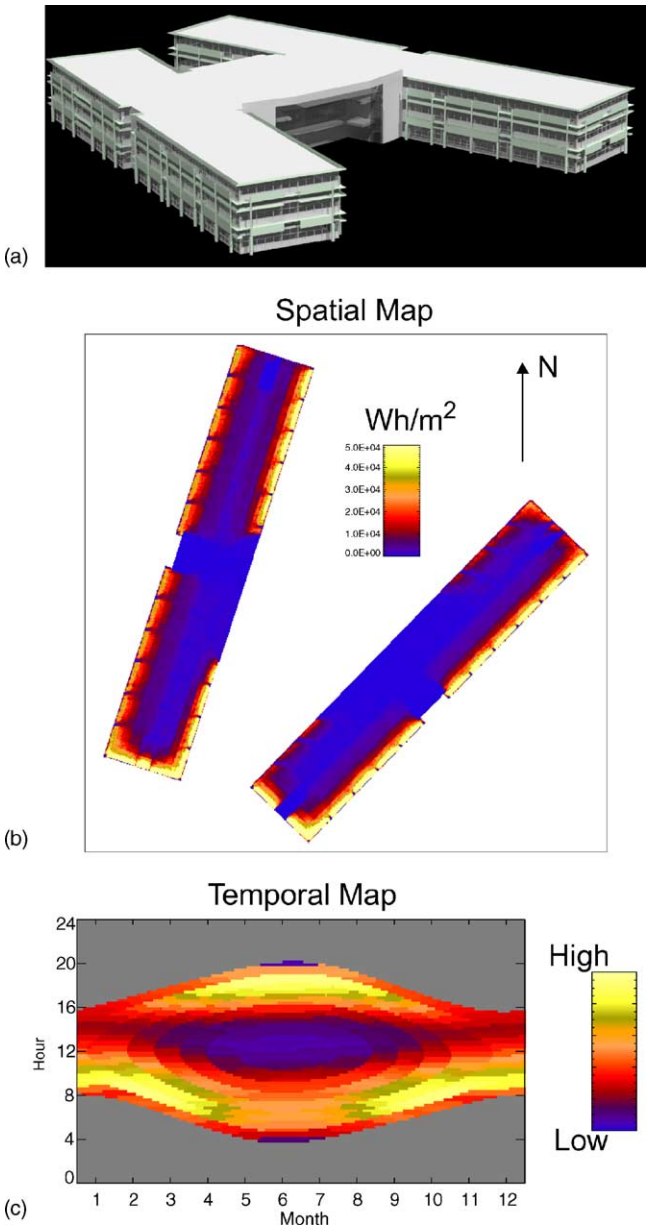

Fig. 3. Rendering and STIMAP analysis of building with brise-soleil.

equations [6]. The locale used for the pseudo-Changi example described below was the Midlands, UK. Any geographical location could be used, the only requirement is a suitable TRY dataset. Although a time-step of 1 h is usual for TRYs, a 15 min time-step for sun positions is used as the default to ensure a smooth distribution. The sun positions for the Midlands, UK are shown in Fig. 4a. The distribution in altitude and azimuth is divided into 'bins' using a grid of arbitrary resolution. Here a grid size of 8° was used for both angles. This bin size is commensurate with a time-step of approximately half an hour (because the sun traverses an arc of 15° every hour). The number of sun positions that occurred in each bin are counted, and the bin-mean sun position evaluated (Fig. 4b). The number counted for each bin is indicated by shade (see adjacent legend), and the bin-mean position is marked by a cross (×). For this combination of locale and bin size, there were 179 bins that contained one or more sun positions. A series of 179 irradiance renderings showing the floor plan are then computed—one each with a unit radiance sun at the bin-mean sun position. A good position to 'view' the floor plan is from high above its approximate mid-point. This is the position of the 'virtual camera' for the renderings. From this vantage point, it is possible to 'see through' the roof of the building by applying the forward clipping plane in *Radiance*. This eliminates all visible surfaces in front of the vantage point to a set distance without interfering with the simulation of the propagation of light. The total annual irradiation image due to all the sun conditions in the TRY is synthesised from these 179 irradiance renderings.

For any fixed (*or almost fixed*) configuration of self-radiant entities (i.e. sun) in a scene, an irradiation image of the scene is equal (*or almost equal*) to the normalised irradiation image multiplied by the magnitude of the radiant output of the source configuration. For example, the irradiation image I_p^{sun} for a scene 'lit up' by a sun of radiance R_p^{sun} is given by

$$I_p^{\text{sun}} = N_b^{\text{sun}} R_p^{\text{sun}} \, \Delta t \tag{1}$$

where N_b^{sun} is the normalised irradiance image for the scene computed using a sun of unit radiance at position b, and Δt is the integration period, i.e. the time-step used for the distribution shown in Fig. 4. The actual sun position p needs to be at *or near to* the position b. Here, the position b is the bin-mean position and *or near to* applies to all those sun positions in that bin. Note that the irradiation image is simply the normalised irradiance image (an array) multiplied by the product of two scalars. It is possible to synthesise an irradiation image for each time-step of the TRY using Eq. (1) and then sum the images to give an image for the total annual irradiation. This total however, can be computed far more efficiently by first evaluating bin-totals on a bin by bin basis as follows. The bin-total irradiation image for bin b is

$$I_b^{\text{sun}} = n_b \, \Delta t N_b^{\text{sun}} \sum_{p \in b} R_p^{\text{sun}} \tag{2}$$

where R_p^{sun} is the solar radiance for position p and N_b^{sun} is the normalised irradiance image for bin b. Here, b is also used to denote the set of positions p for that bin, and n_b is the number of elements (i.e. positions) in the set. Note that the summation is simply the arithmetic total of the sun radiances for all the sun positions in bin b and so accounts for *all* the varying sun conditions for that bin, e.g. clear, cloudy, hazy, etc. Also, it is a simple matter to synthesise a time-series of the instantaneous direct irradiance averaged across the floor plan. This quantity will be needed to determine the peak solar cooling load.

The solar radiance values for this analysis were derived from the direct normal irradiance time-series of the Kew TRY, Fig. 5. The hourly values of the TRY were interpolated

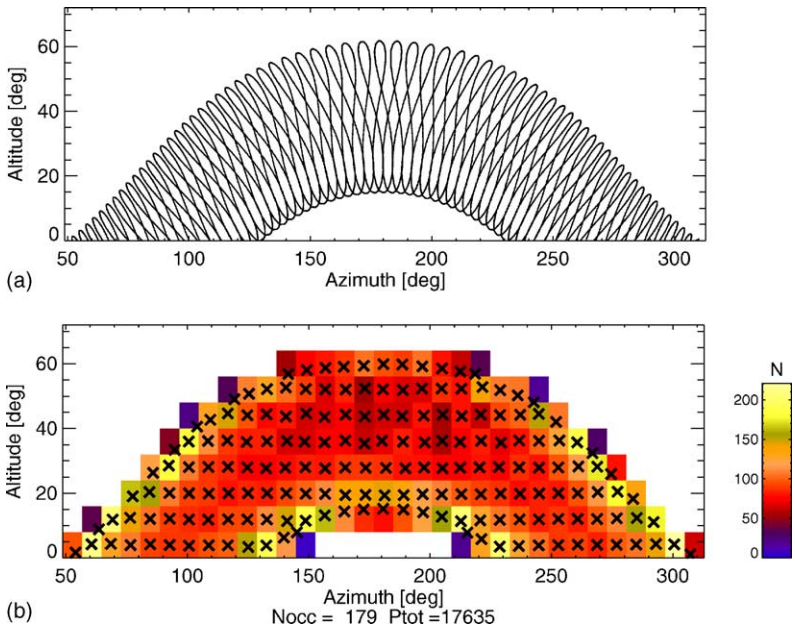

Fig. 4. Procedure to determine the sun position for the sun and the anisotropic sky renderings from the distribution of annually occurring sun positions (15 min time-step).

to a 15 min time step to match that used for the distribution in sun positions (Fig. 4). The irradiation image total I_T^{sun} for the entire year is computed by summing the bin-totals for all the bins in the distribution as follows:

$$I_T^{\text{sun}} = \sum_{b=1}^{B} I_b^{\text{sun}} \tag{3}$$

For the distribution shown in Fig. 4, the number of bins $B = 179$. Annual totals of irradiation are the most straightforward to derive using this method. However, the summation can easily be modified to produce a total for any desired fraction of the year, e.g. seasonal totals, monthly totals, a.m. and p.m. totals, etc.

The computation times for the renderings are very short because only direct irradiation is modelled. The set of 179 renderings for each unique roof design takes only about 10–15 min, and the entire run for 42 cases only a few hours (Apple iMac, 800 MHz, G4).

3. Parametrically defined shading systems

3.1. The pseudo-Changi model

The building model used to demonstrate the new approach was inspired by the concept rendering of Changi Terminal 3 (Fig. 2). The form of the scheme used to orientate the fins was not known, and the final design may differ from that shown in the concept rendering. Accordingly, the model devised for this paper is referred to as "pseudo-Changi".

A parametrically defined shading system is one where a key property of the system (e.g. fin orientation) is governed by some rule (i.e. equation). The geometry of the shading system is then generated using the rule. It is often a simple matter to change one or more parameters of the rule which allows the possibility for generating any number of variants of the original design. The roof structure of the pseudo-Changi model comprised 3600 shading fins positioned just under a double-glazed roof. Each fin was 3 m

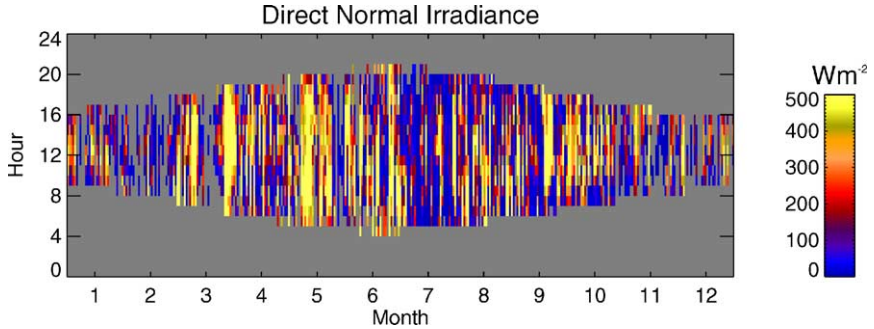

Fig. 5. Test reference year time-series for direct normal irradiation. The time-series of 8760 hourly values is shown as a 365 days by 24 h array.

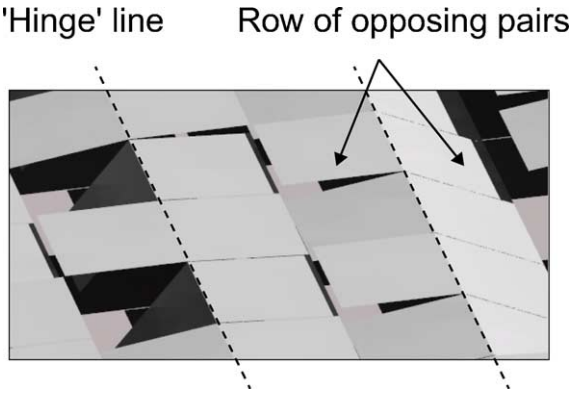

Fig. 6. Close-up of pseudo-Changi roof.

square, though the absolute dimensions are not relevant for the purpose of demonstration. The fins were arranged in rows of opposing pairs, i.e. ones that shared the same 'hinge', Fig. 6.

3.2. Parametric scheme

The rest position for each of the shading fins was 0° to the horizontal, i.e. fully 'closed'. The fin was displaced from rest (i.e. 'opened') depending on the magnitude of a (uniform) random number. A probability factor governed the likelihood that a fin would be opened for any given random number. The probability factor applied to the shading fins was one design parameter, the other was the overall orientation of the roof which was varied from 0 to 180° in steps of 30°. A preferred design for shading systems of this type may be to have fins on one side of the hinge that are more open than those on the other. This allows the possibility for aspects not prone to solar penetration to be more open for the provision of daylight (Fig. 7).

The parametric scheme for displacing the fins was as follows. For the rows of fins initially on the north side of the hinge

$$\begin{aligned} &\text{if } (x < 0.3), && \text{then } \theta_n = 0^\circ \\ &\text{if } ((x \geq 0.3) \text{ and } (x < V)), && \text{then } \theta_n = 4^\circ \\ &\text{if } (x \geq V), && \text{then } \theta_n = 25^\circ \end{aligned}$$

where x is a uniform random number in the range 0–1, and V is a probability factor in the range 0.4–0.9. This factor was fixed for each of the design variants. For the rows of fins initially on the south side of the hinge

$$\begin{aligned} &\text{if } (x < 0.3), && \text{then } \theta_s = 0^\circ \\ &\text{if } ((x \geq 0.3) \text{ and } (x < V)), && \text{then } \theta_s = 8^\circ \\ &\text{if } (x \geq V), && \text{then } \theta_s = 50^\circ \end{aligned}$$

With this scheme, there is a probability of 0.3 that the fins on either side of the hinge remain closed. For $V = 0.4$, there is a probability of 0.1 that the fin will be opened to 4° and a probability of 0.6 that it will be opened to 25° (for θ_n, the fin initially on the north side of the hinge). The design variant where $V = 0.4$ has the highest probability of 'open' shading fins, and the one where $V = 0.9$ has the lowest probability.

Renderings showing the view of the roof shading system from above together with the pattern of solar penetration on the floor for one sun position are given in Fig. 8. Note the clumping pattern visible in the arrangement of the fins and the shadow pattern on the floor. Computation of the total annual direct irradiation was carried out for all combinations of six probability factors (0.4–0.9 in steps of 0.1) and seven orientations (0–180° in steps of 30°). The results are presented in Section 4.

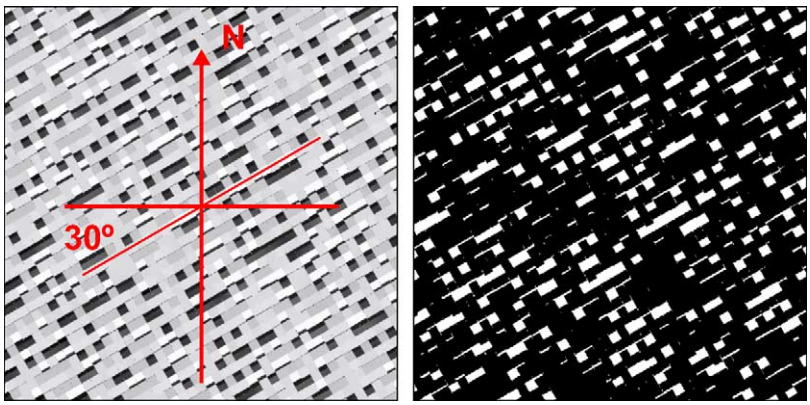

Fig. 7. Fins in rows of opposing pairs.

Fig. 8. Renderings showing views of the shading system and the pattern of solar penetration on the floor (one sun position).

Table 1
Total annual solar irradiation averaged across floor area (kWh/m^2) for all 42 design variants

Orientation (°)	Probability factor					
	0.4	0.5	0.6	0.7	0.8	0.9
TAI						
0	62.7	55.7	47.9	40.5	29.9	19.8
30	59.8	53.1	44.8	37.5	29.8	18.2
60	53.3	*46.0*	43.5	35.1	*26.2*	16.9
90	47.1	41.9	37.2	30.4	23.9	15.3
120	41.1	36.8	32.7	28.4	20.5	12.5
150	35.7	33.1	29.6	24.9	18.2	10.7
180	34.0	32.2	29.4	24.5	19.2	11.1

Table 2
Peak instantaneous solar gain averaged across floor area (W/m^2) for all 42 design variants

Orientation (°)	Probability factor					
	0.4	0.5	0.6	0.7	0.8	0.9
PII						
0	124	107	88	73	52	35
30	122	110	87	72	56	33
60	126	*102*	94	73	*52*	32
90	122	100	92	66	50	32
120	116	100	87	68	47	30
150	96	85	69	55	39	24
180	70	65	56	45	35	20

4. Results

Spatial and temporal irradiation maps were produced for each of the 42 variants for the roof shading system. The total annual irradiation averaged across the floor area was determined from the irradiation images. This single value characterises the overall performance of each variant of the shading system in terms of solar radiation incident on the floor, Table 1.

The results in Table 1 reveal the precise relation between the two design parameters (probability factor and orientation) and the total annual irradiation. The peak instantaneous irradiance (PII) averaged across the floor area was also determined (Table 2).

Irradiation images for two of the design variants are shown in Fig. 9 together with renderings giving a view from above of the shading fin array (these two variants are identified in Tables 1 and 2 with italicised values in the table cell). Evident in the irradiation maps are the 'clumpy' patches that result from the random scheme used to define the arrangement of the shading fins. Two such patches are marked on one of the irradiation images (Fig. 9). For this design variant, the total annual irradiation averaged across the entire floor area was 46 kWh/m^2 (Table 1). Averaged across the 'coolspot' region A and the 'hotspot' region B, the total annual irradiation was 24 and 66 kWh/m^2, respectively. The propensity for solar penetration with this design variant is shown in Fig. 10a (similar scale as Fig. 3c). The highest levels of solar penetration are likely to occur between the hours of 9:00–12:00 h during the months May–August. The temporal maps for just the 'coolspot' and 'hotspot' regions show that the patterns of exposure to solar penetration are very different from the area as a whole. The 'coolspot' (region A) is likely to receive direct solar radiation before 9:00 h during the summer months, and between 10:00 and 14:00 h during early spring and late autumn (Fig. 10b). Whereas the 'hotspot' (region B) has a high propensity for direct solar penetration from 8:00 to 13:00 h from March to October (Fig. 10c).

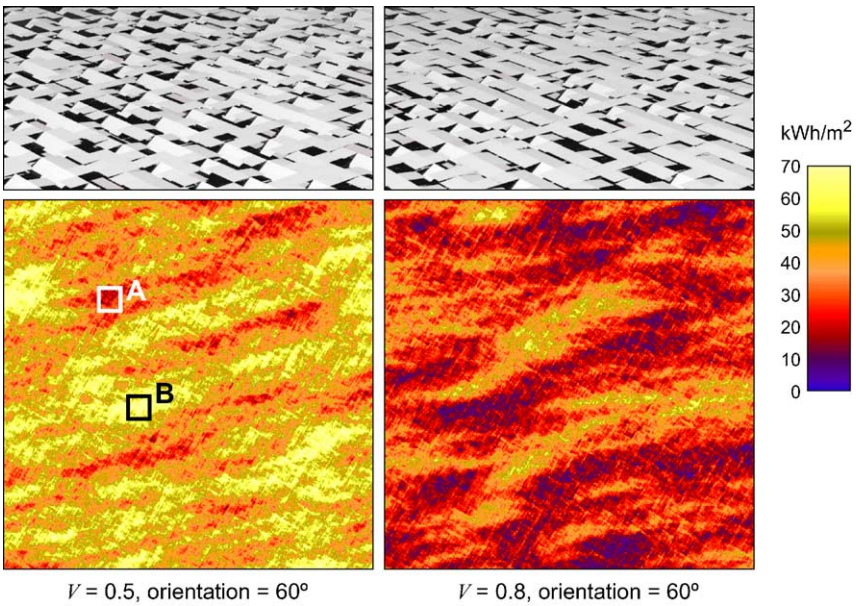

Fig. 9. Rendering of shading fin configuration and image of total annual irradiation for two variants.

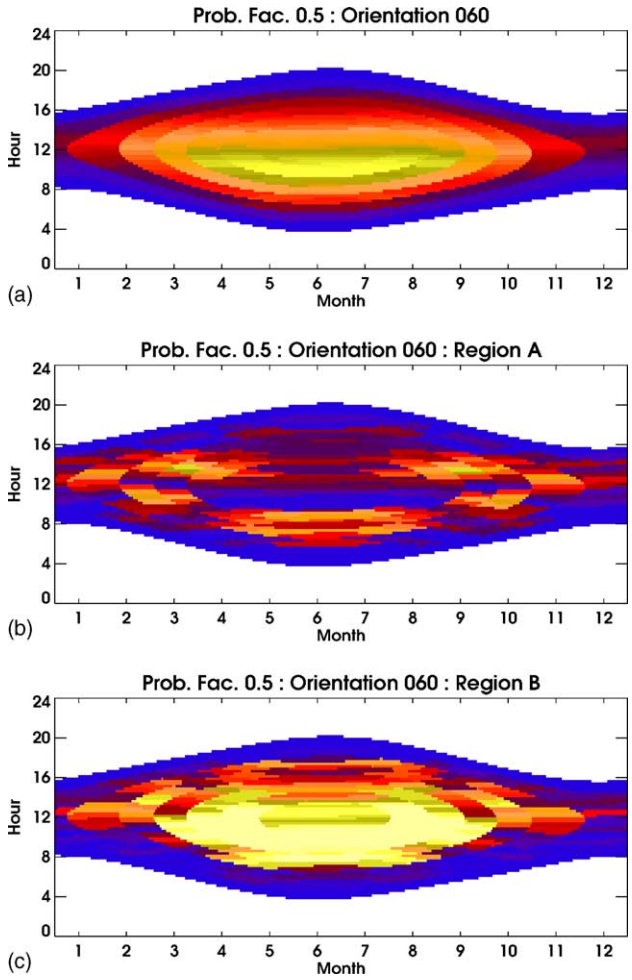

Fig. 10. Temporal maps.

5. Discussion

The analysis has demonstrated the relative ease and speed with which a large number of design variants of a complex shading system can be evaluated in terms of the spatial and temporal dynamics of direct solar penetration. As noted, the pseudo-Changi roof example was used solely to showcase the new technique. The design parameters and performance specification for the actual Changi roof were not known, so no attempt was made to guess what they might be. The clumpy patterns in total annual irradiation that result from the parametric scheme present some interesting design possibilities (Fig. 9). For example, the areas of high total annual irradiation could be used to locate the trees and planting that the architects envisage for this building (Fig. 2).

Protection from direct solar penetration is one part of the design specification for a shading system. The provision of adequate daylight is another key function. The author has demonstrated the accurate prediction of time-varying internal illuminances based on the same meteorological data used here to predict total annual irradiation [7]. In a full-blown performance analysis, the design of the roof shading system could be tailored with some precision to balance the competing requirements of solar protection and daylighting.

The new technique can of course be used to image any building surface including the shading devices themselves. This could be used to optimise the design of complex shading structures by identifying those parts of the structure that experience low levels of irradiation, i.e. possibly redundant structure that adds little to the overall shading of the building. If required, views showing the floor and walls together could be rendered using ‘fish-eye’ view parameters from a vantage point just below the ceiling. Total annual irradiation images for these views would be computed as before.

When detailed comparisons are required to fine-tune a design, a technique called difference mapping can be applied to pairs of both the spatial and the temporal maps. A different map is simply one spatial (or temporal map) subtracted from another. The difference maps disclose precisely how one design performs relative to another in terms of where (spatial difference) and when (temporal difference) solar penetration occurs.

In terms of the precision and scope of the analysis, and the swiftness of the computation, it is hard to see how a physical (i.e. scale) model approach could rival the evaluation presented here.

6. Conclusion

The shading analysis described here offers a marked advance over traditional, largely qualitative, methods. The new technique can be applied to very complex shading systems, working either directly with 3D CAD models, or as shown here, using parametrically defined geometries. The images showing total annual irradiation are easy to interpret and disclose much greater information on overall shading performance than the more numerous, but qualitative, shadow-pattern images of the conventional method. The normalised irradiance images can be processed to produce irradiation images and/or numerical data on virtually any spatio-temporal aspect of direct solar penetration. The reduction of data to summary metrics allows for the reliable comparison of any number of design variants.

Acknowledgements

Rob Shakespeare (Indiana University, USA) created the 3D model used in Fig. 1. The author wishes to thank Architects Stephen George & Partners (Leicester, UK) for permission to use the building model shown in Fig. 1. The movie sequence used in Fig. 1 can be down-loaded from http://www.iesd.dmu.ac.uk/∼jm/sg98jm.mov.

References

[1] BRE Designing with Innovative Daylighting Building Research Establishment Report BR302, 1996.
[2] G. Ward Larson, R. Shakespeare, Rendering with Radiance: The Art and Science of Lighting Visualization, Morgan Kaufmann, San Francisco, 1998.
[3] J. Mardaljevic, A new image-based technique to predict solar penetration, in: Proceedings of the CIBSE National Conference, July 2001.
[4] Energie Solar Shading for the European Climates Energy Research Group, University College Dublin, European Commission Report, 2000, http://erg.ucd.ie/mb_shading_systems.pdf.
[5] J. Mardaljevic, The BRE-IDMP dataset: a new benchmark for the validation of illuminance prediction techniques, Lighting Res. Technol. 33 (2) (2001) 117–136.
[6] P. Tregenza, S. Sharples, Daylighting Algorithms ETSU S/1350, 1993.
[7] J. Mardaljevic, The simulation of annual daylighting profiles for internal illuminance, Lighting Res. Technol. 32 (3) (2000) 111–118.